Title	Finite-element-based generalized impedance boundary condition for modeling plasmonic nanostructures
Author(s)	He, S; Sha, WEI; Jiang, L; Choy, WCH; Chew, WC; Nie, Z
Citation	IEEE Transactions On Nanotechnology, 2012, v. 11 n. 2, p. 336-345
Issued Date	2012
URL	http://hdl.handle.net/10722/146870
Rights	Creative Commons: Attribution 3.0 Hong Kong License

Finite-Element-Based Generalized Impedance Boundary Condition for Modeling Plasmonic Nanostructures

Shiquan He, *Student Member, IEEE*, Wei E. I. Sha, *Member, IEEE*, Lijun Jiang, *Member, IEEE*, Wallace C. H. Choy, *Senior Member, IEEE*, Weng Cho Chew, *Fellow, IEEE*, and Zaiping Nie, *Senior Member, IEEE*

***Abstract*—The superior ability of plasmonic structures to manipulate light has propelled their extensive applications in nanophotonics techniques and devices. Computational electromagnetics plays a critical role in characterizing and optimizing the nanometallic structures. In this paper, a general numerical algorithm, which is different from the commonly used discrete dipole approximation, the finite-difference time-domain, and the surface integral equation (SIE) method, is proposed to model plasmonic nanostructures. In this algorithm, the generalized impedance boundary condition (GIBC) based on the finite element method (FEM) is formulated and converted to the SIE. The plasmonic nanostructures with arbitrary inhomogeneity and shapes are modeled by the FEM. Their complex electromagnetic interactions are accurately described by the SIE method. As a result, the near field of plasmonic nanostructures can be accurately calculated. The higher order basis functions, together with the multifrontal massively parallel sparse direct solver, are involved to provide a higher order accurate and fast solver.**

***Index Terms*—Boundary integral equation (BIE), finite element method (FEM), generalized impedance boundary condition (GIBC), plasmonic nanostructures.**

I. Introduction

PROGRESS in the field of nanotechnology has greatly propelled the experimental investigation and exploitation of novel effects at the nanoscale. Due to the unique features of plasmons, such as the tunable resonance and the near-field enhancement, it has wide applications in biosensing, clean energy, and spectroscopy [1]–[5]. Computational electromagnetics (CEM) plays a critical role in characterizing and optimizing plasmonic structures. An accurate, fast, and efficient CEM solver can help to understand the working principles of the plasmonic nanostructure better, reduce the experimental cost, and shorten the development period [6], [7]. Full-wave electromagnetic solvers based on Maxwell's equations are indispensable to accurately predict the light–matter interaction in nanostructures. Available numerical methods for modeling the plasmonic effects can be mainly classified into three types: 1) semianalytical methods [such as T-matrix method and multiple multipole method (MMP)] [8], [9]; 2) the differential equation (DE) methods [such as finite-difference time-domain method and finite element method (FEM)] [10]–[12]; and 3) the integral equation (IE) methods [such as volume IE and surface IE (SIE)] [13]–[20].

T-matrix [8] is a powerful method for modeling well-separated nanoparticles only if the solution of each particle is known, and the MMP [9] depends on the fundamental multipole expansion. They potentially yield an ill-conditioned system when extended to model arbitrarily shaped nanostructures.

The DE method generates a sparse matrix. Hence, its cost of the computer storage and CPU time is at $O(N)$ per iteration in iterative solvers, where N is the number of unknowns. Thanks to the volumetric grids it employs, it is convenient for analyzing the near-field responses. However, other than the scatterer, the surrounding free-space volume also must be discretized for the absorption boundary condition (ABC) setups [21], [22]. The spurious reflections from the ABC will degrade the accuracy of the simulation results. Furthermore, the dispersion error of both FEM and FDTD methods and the staircased approximation of the FDTD method all decrease the modeling accuracy for the high-contrast plasmonic structures with strong evanescent wave coupling.

Different from DE methods, IE methods only discretize the scattering objects and can satisfy the radiation boundary condition automatically. Hence, they usually have higher accuracy compared with DE methods. Nevertheless, a full dense matrix from them is costly for computer resources. Fortunately, fast algorithms, such as the fast Fourier transform [23] and the multilevel fast multipole algorithm (MLFMA) [24], have been successfully developed to reduce the computational complexity. As mentioned in the previous work [20], the discrete dipole approximation (DDA) [15] breaks down in capturing the plasmonic physics while the SIE (also named as boundary element

Manuscript received January 3, 2011; revised July 3, 2011; accepted October 4, 2011. Date of publication November 15, 2011; date of current version March 9, 2012. This work was supported in part by the International Joint Research Project of China ("111Project," under contract B07046), National Natural Science Foundation of China (Contract No. 60931004) and partially by the Hong Kong Government under Research Grants Council, Ref. Nos. 711508 and 711609; ITF, No. ITS/159/09. The review of this paper was arranged by Associate Editor S. Assefa.

S. He and Z. Nie are with the University of Electronic Science and Technology of China, Chengdu 610054, China (e-mail: shiquanhe@uestc.edu.cn; zpnie@uestc.edu.cn).

W. E. I. Sha, W. C. H. Choy, and W. C. Chew are with the University of Hong Kong, Hong Kong (e-mail: shawei@hku.hk; chchoy@eee.hku.hk; wcchew@hku.hk).

L. Jiang is with the University of Hong Kong, Hong Kong, and also with the IBM T. J. Watson Research Center, Yorktown Heights, NY 10598 USA (e-mail: jianglj@hku.hk).

Color versions of one or more of the figures in this paper are available online at http://ieeexplore.ieee.org.

Digital Object Identifier 10.1109/TNANO.2011.2171987

method (BEM) [16] or boundary IE (BIE) [17] in electromagnetics) is recommended to model plasmonic nanostructures. Due to the "surface" triangulation, the SIE method produces much smaller unknowns. However, it can only be employed to simulate the homogenous or piecewise-constant targets. For the arbitrary inhomogeneity or more complex environment encountered in plasmonic nanodevices, the numerical implementation of the SIE method is essential but difficult. Particularly, the SIE method is not efficient for the near-field calculation, which is critical for understanding the fundamental physics or device-related physics of plasmonic nanostructures. For each given near-field point, one has to conduct a surface integration. If the observation region is large or too many sample points are required for resolving the near-field distribution, the relevant calculations will be too expensive. In addition, the fast algorithms cannot accelerate the "near-field" calculation due to the singularity of the dyadic Green's function.

All of the aforementioned algorithms have their pros and cons in the plasmonic nanostructure simulation. In this paper, we hybridize the SIE and FEM to avoid their drawbacks. Their advantages are preserved while drawbacks are removed. A rigorous, efficient, and general electromagnetic method is thereby developed to model the plasmonic nanostructures.

The equivalence principle [25] uses the equivalent or fictitious sources to reproduce the same field within a region of interest. Even for the inhomogeneous structures embedded in a homogenous background, the SIE still can be employed for the exterior field calculation by using the equivalent sources $\mathbf{J}_s(=\hat{n}\times\mathbf{H})$ and $\mathbf{M}_s(=-\hat{n}\times\mathbf{E})$. Here, $\mathbf{J}_s$ ($\mathbf{M}_s$) is the electric (magnetic) current on the surfaces of inhomogeneous structures, and $\mathbf{E}$ ($\mathbf{H}$) is the related electric (magnetic) field. To guarantee the unique solution of the SIE, a generalized impedance boundary condition (GIBC) [26] based on the FEM is derived to establish a universal relation between the electric current and the magnetic current, i.e., $\mathbf{M}_s(\mathbf{r})=\mathbf{Z}(\mathbf{r},\mathbf{r}')\mathbf{J}_\mathbf{s}(\mathbf{r}')$ using extended Einstein notation. Then, a reduced SIE only involving the equivalent electric current $\mathbf{J}_s$ is obtained. Finally, the MLFMA [27] is used to accelerate the solution of the SIE. In addition, the second-order basis functions [28] and the multifrontal massively parallel sparse direct solver (MUMPS) [29] are introduced in our algorithm to achieve higher order accuracy and fast calculation of the generalized impedance operator $\mathbf{Z}(\mathbf{r},\mathbf{r}')$.

Different from the conventional finite element-BIE [30]–[32] method, the proposed method is applicable to multiregion electromagnetic (EM) problems. We only need to precompute the inverse of several stiffness-mass submatrices, but not the whole one. The proposed method also distinguishes from the FEM–BEM in [33]–[35]. For our method, the tangential continuities of $\mathbf{E}$ and $\mathbf{H}$ fields across the interfaces between FEM and BEM regions are imposed directly. Furthermore, only equivalent electric current $\mathbf{J}_s$ on the FEM–BEM interface is introduced. Due to the GIBC (to be derived in Section II of this paper), a sparse matrix with smaller size for each region is inverted to transfer the original unknowns to the unknowns on the equivalent surface. The dimension of the final impedance matrix becomes much smaller than that in [35] as well. For very complicated structures with strong coupling, the iteration methods are hard to converge to an accurate solution. Reducing the dimension of final matrix can greatly help the Krylov subspace iteration or the direct LU decomposition [36]. As far as we know, it is the first time that a hybrid GIBC-FEM method has been used to model the plasmonic nanostructures.

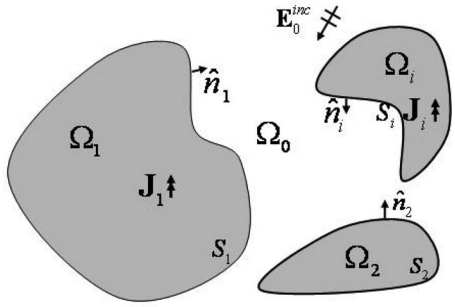

Fig. 1. General arbitrary inhomogeneous problem.

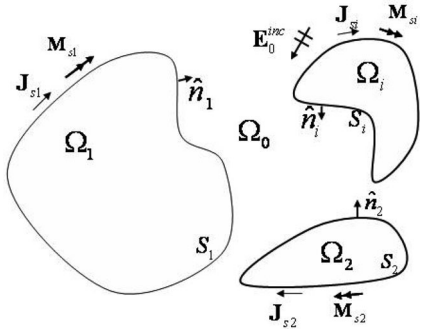

Fig. 2. Love equivalence model for the exterior region.

The rest of this paper is organized as follows. In Section II, the BIE will be established on the surface of each nanoparticle or each fictitious surface. The finite-element-based GIBC is formulated for arbitrary inhomogeneous and anisotropic mediums in Section III. Section IV shows the numerical implementation to solve the final BIE. Through numerical discretization, the mathematical representation of Maxwell's equations is converted to a set of matrix equations. The proposed method is applied to model plasmonic nanostructures in Section V. Section VI summarizes the contributions of this paper.

II. BIE

We consider several inhomogeneous structures embedded in a homogeneous background. As illustrated in Fig. 1, each inhomogeneous region and its boundary are represented by domain Ω_i and boundary S_i, $i=1, 2, \ldots, N$, where N is the number of inhomogeneous regions. The homogenous background is defined as Ω_0. Here, S_i can be the geometric boundary of an object or a fictitious boundary which encloses this object. According to the Love equivalence principle [8], [25], [37] as shown in Fig. 2, no matter what material it is, the inner inhomogeneity can be removed and filled with the homogeneous background for the exterior equivalence. Then, the EM field in Ω_0 will be generated by the radiation of equivalent sources $\mathbf{J}_{si}$ and $\mathbf{M}_{si}$ located on S_i expressed by $\mathbf{J}_{si}=\hat{n}_i\times\mathbf{H}_0$ and $\mathbf{M}_{si}=-\hat{n}_i\times\mathbf{E}_0$. Here,

$\mathbf{E}_0$ and $\mathbf{H}_0$ are the total field at Ω_0, and $\hat{n}_i$ denotes the outward unit normal vector.

The total field can be expressed as the summation of the incident field and the scattered field

$$\mathbf{E}_0(\mathbf{r}) = \mathbf{E}_0^{\text{inc}}(\mathbf{r}) + \mathbf{E}_0^{\text{sca}}(\mathbf{r}) \tag{1}$$

$$\mathbf{H}_0(\mathbf{r}) = \mathbf{H}_0^{\text{inc}}(\mathbf{r}) + \mathbf{H}_0^{\text{sca}}(\mathbf{r}) \tag{2}$$

and

$$\mathbf{E}_0^{\text{sca}}(\mathbf{r}) = \eta_0 \mathtt{L}\left(\sum_{i=1}^{N} \mathbf{J}_{si}\right) - \mathtt{K}\left(\sum_{i=1}^{N} \mathbf{M}_{si}\right) \tag{3}$$

$$\mathbf{H}_0^{\text{sca}}(\mathbf{r}) = \frac{1}{\eta_0}\mathtt{L}\left(\sum_{i=1}^{N} \mathbf{M}_{si}\right) + \mathtt{K}\left(\sum_{i=1}^{N} \mathbf{J}_{si}\right). \tag{4}$$

Here, $\mathtt{L}(\cdot)$ and $\mathtt{K}(\cdot)$ are integral operators defined by (the time convention $e^{-i\omega t}$ is assumed)

$$\mathtt{L}(\mathbf{X}) = ik_0 \int_S \bar{\mathbf{G}}(\mathbf{r}, \mathbf{r}') \bullet \mathbf{X}(\mathbf{r}') d\mathbf{r}', \quad \mathbf{r}' \in \cup S_i \tag{5}$$

$$\mathtt{K}(\mathbf{X}) = \int_S \nabla G(\mathbf{r}, \mathbf{r}') \times \mathbf{X}(\mathbf{r}') d\mathbf{r}', \quad \mathbf{r}' \in \cup S_i \tag{6}$$

$$G(\mathbf{r}, \mathbf{r}') = \frac{e^{ik_0|\mathbf{r}-\mathbf{r}'|}}{4\pi|\mathbf{r}-\mathbf{r}'|} \tag{7}$$

$$\bar{\mathbf{G}}(\mathbf{r}, \mathbf{r}') = \left(\bar{\mathbf{I}} + \frac{\nabla\nabla}{k_0^2}\right) G(\mathbf{r}, \mathbf{r}'). \tag{8}$$

Here, $G(\mathbf{r}, \mathbf{r}')$ and $\bar{\mathbf{G}}(\mathbf{r}, \mathbf{r}')$ denote the scalar and dyadic Green's function in the homogeneous background, and k_0 and η_0 represent the wave number and wave impedance in the region Ω_0, respectively.

According to the extinction theorem, four fundamental BIEs can be established at each boundary S_i [18], [38]

TE formulation

$$\left[\mathbf{E}_0^{\text{inc}} + \eta_0 \mathtt{L}\left(\sum_{i=1}^{N} \mathbf{J}_{si}\right) - \mathtt{K}\left(\sum_{i=1}^{N} \mathbf{M}_{si}\right)\right]_{\tan} = 0, \quad \mathbf{r} \in S_i^-. \tag{9}$$

TH formulation

$$\left[\mathbf{H}_0^{\text{inc}} + \frac{1}{\eta_0}\mathtt{L}\left(\sum_{i=1}^{N} \mathbf{M}_{si}\right) + \mathtt{K}\left(\sum_{i=1}^{N} \mathbf{J}_{si}\right)\right]_{\tan} = 0, \quad \mathbf{r} \in S_i^-. \tag{10}$$

NE formulation

$$\hat{n}_i \times \left[\mathbf{E}_0^{\text{inc}} + \eta_0 \mathtt{L}\left(\sum_{i=1}^{N} \mathbf{J}_{si}\right) - \mathtt{K}\left(\sum_{i=1}^{N} \mathbf{M}_{si}\right)\right] = 0, \quad \mathbf{r} \in S_i^-. \tag{11}$$

NH formulation

$$\hat{n}_i \times \left[\mathbf{H}_0^{\text{inc}} + \frac{1}{\eta_0}\mathtt{L}\left(\sum_{i=1}^{N} \mathbf{M}_{si}\right) + \mathtt{K}\left(\sum_{i=1}^{N} \mathbf{J}_{si}\right)\right] = 0, \quad \mathbf{r} \in S_i^-. \tag{12}$$

where S_i^- denotes the inner side of boundary $S_i (i = 1, 2, \ldots, N)$.

The four formulations indicate that given the field distribution $\mathbf{E}_0$ and $\mathbf{H}_0$ in the exterior region, the equivalent sources $\mathbf{J}_{si}$ and $\mathbf{M}_{si}$ will generate the right field $\mathbf{E}_0$ and $\mathbf{H}_0$ if $\mathbf{J}_{si} = \hat{n} \times \mathbf{H}_0$ and $\mathbf{M}_{si} = -\hat{n} \times \mathbf{E}_0$. These four formulations and their linear combinations give rise to a set of BIEs with unknowns $\mathbf{J}_{si}$ and $\mathbf{M}_{si}$. However, at the boundary S_i, four formulations depend on each other. Hence, they are not sufficient to derive a unique solution of $\mathbf{J}_{si}$ and $\mathbf{M}_{si}$. The field distribution or boundary conditions within the inner regions should be taken into account. A combined BIE can be written as

$$\alpha_i(9) + \beta_i(10) + \gamma_i(11) + \chi_i(12) = 0, \quad \mathbf{r} \in S_i^- \tag{13}$$

where α_i, β_i, γ_i, and χ_i are the combination coefficients; the integer subscripts represent the left-hand side of (9)–(12). There are many different forms for different coefficients. For example, the well-known combined field IE [38] that can avoid the internal resonance can be obtained by setting $\beta_i = 0$, $\gamma_i = 1 - \alpha_i$, and $\chi_i = 0$, $\alpha_i \in [0, 1]$.

Equation (13) has established a connection between the equivalent magnetic current $\mathbf{M}_{si}$ and the equivalent electric current $\mathbf{J}_{si}$ implicitly. To uniquely determine the values of $\mathbf{J}_{si}$ and $\mathbf{M}_{si}$, another boundary condition between them is required. If a GIBC is established as $\mathbf{M}_{si}(\mathbf{r}) = \mathbf{Z_i}(\mathbf{r}, \mathbf{r}')\mathbf{J_{si}}(\mathbf{r}')$, then it can be used in (13) to get a reduced equation only involving unknown $\mathbf{J}_{si}$. Consequently, the solution can be determined. In our previous work, a GIBC based on the PMCHWT like SIE has been utilized to simulate conductor with finite conductivity [26]. In the following sections, we will demonstrate how to formulate the GIBC based on the FEM for arbitrary inhomogeneous medium.

III. Finite-Element-Based GIBC

A. Finite Element Discretization

According to Maxwell's curl equations

$$\nabla \times \mathbf{E}_i = i\omega\mu_0\bar{\mu}_{ri} \bullet \mathbf{H}_i \tag{14}$$

$$\nabla \times \mathbf{H}_i = \mathbf{J}_i - i\omega\varepsilon_0\bar{\varepsilon}_{ri} \bullet \mathbf{E}_i \tag{15}$$

one can get the vector wave equation in each region

$$\nabla \times \bar{\mu}_{ri}^{-1} \bullet \nabla \times \mathbf{E}_i - k_0^2\bar{\varepsilon}_{ri} \bullet \mathbf{E}_i = ik_0\eta_0\mathbf{J}_i, \quad \mathbf{r} \in \Omega_i \tag{16}$$

where $\bar{\varepsilon}_{ri}$ and $\bar{\mu}_{ri}$ are the permittivity and the permeability in Ω_i, respectively, $\mathbf{J}_i$ represents the excitation source in this region, and $\mathbf{E}_i$ and $\mathbf{H}_i$ are the electric and magnetic fields, respectively.

According to the uniqueness theorem, the field can be uniquely determined by the governing equations and related boundary conditions. The commonly used boundary conditions are given by

$$\hat{n}_i \times \mathbf{E}_i = -\mathbf{M}_{si} \text{ on } S_i \tag{17}$$

or

$$\hat{n}_i \times \mathbf{H}_i = \mathbf{J}_{si} \text{ on } S_i. \tag{18}$$

If $\mathbf{M}_{si} = 0$, (17) gives a perfect electric conductor (PEC) boundary condition. The PEC boundary condition can be implemented easily by decreasing the number of unknowns at the boundary. Since any object is penetrable in nanooptics, we mainly consider the natural boundary condition shown in (18) in this paper.

The FEM converts the boundary value problem (16)–(18) to an optimization process of the functional

$$F(\mathbf{E}_i) = \frac{1}{2}\int_{\Omega_i}\left[(\nabla\times\mathbf{E}_i)\bullet\bar{\mu}_{ri}^{-1}\bullet(\nabla\times\mathbf{E}_i) - k_0^2\mathbf{E}_i\bullet\bar{\varepsilon}_{ri}\bullet\mathbf{E}_i\right]dV - ik_0\eta_0\int_{\Omega_i}\mathbf{E}_i\bullet\mathbf{J}_i dV + ik_0\eta_0\int_{s_i}\mathbf{E}_i\bullet\mathbf{J}_{si}dS. \quad (19)$$

Here, subwavelength tetrahedrons and triangular patches are utilized to discretize the domain Ω_i and its boundary S_i, respectively. Then, the inner electric field $\mathbf{E}_i$ and the boundary equivalent source $\mathbf{U}_i$ or $\mathbf{J}_{si}$ are represented by the second-order finite element basis functions [28] and RWG basis functions [39]

$$\mathbf{E}_i = \sum_{j=1}^{N_i} e_{ij}\mathbf{N}_{ij} = \{\mathbf{N}_i\}^T\cdot\{e_i\} \quad (20)$$

$$\mathbf{U}_i = ik_0\eta_0\mathbf{J}_{si} = \sum_{j=1}^{L_i} u_{ij}\mathbf{S}_{ij} = \{\mathbf{S}_i\}^T\cdot\{u_i\} \quad (21)$$

where $\{\mathbf{N}_i\} = (\mathbf{N}_{i1}, \mathbf{N}_{i2}, \ldots, \mathbf{N}_{iN_i})^T$, $\{S_i\} = (S_{i1}, S_{i2}, \ldots, S_{iL_i})^T$, $\{e_i\} = (e_{i1}, e_{i2}, \ldots e_{iN_i})^T$, and $\{u_i\} = (u_{i1}, u_{i2}, \ldots, u_{iL_i})^T$. $\mathbf{N}_{ij}$ is the jth finite element basis function in the domain Ω_i, and $\mathbf{S}_{ij}$ is the jth RWG basis function. e_{ij} and u_{ij} denote the weights of each basis function. N_i and L_i are their numbers. According to the variational principle, we can establish a linear equation about $\{e_i\}$ and $\{u_i\}$ by minimizing the functional (19) over the function space$\{\mathbf{N}_i\}$

$$[K_i]\{e_i\} + [B_i]\{u_i\} = \{V_i\}. \quad (22)$$

Here, $[K_i]$ is the stiffness-mass matrix in FEM, $[B_i]$ is a boundary connection matrix, and $\{V_i\}$ is the excitation vector. Each element of them is calculated by

$$[K_i]_{mn} = \int_{\Omega_i}[(\nabla\times\mathbf{N}_{im})\cdot\bar{\mu}_{ri}^{-1}\cdot(\nabla\times\mathbf{N}_{in}) - k_0^2\mathbf{N}_{im}\cdot\bar{\varepsilon}_{ri}\cdot\mathbf{N}_{in}]dV \quad (23)$$

$$[B_i]_{mn} = \int_{S_i}\mathbf{N}_{im}\cdot\mathbf{S}_{in}dS\,,\ \text{i.e.,}\ [B_i] = \{\mathbf{N}_i\}\cdot\{\mathbf{S}_i\}^T \quad (24)$$

$$\{V_i\}_j = ik_0\eta_0\int_{\Omega_i}\mathbf{N}_{ij}\cdot\mathbf{J}_i dV,\ \text{i.e.,}\ \{V_i\} = ik_0\eta_0\{\mathbf{N}_i\}\cdot\mathbf{J}_i. \quad (25)$$

Equation (22) gives a connection between the boundary equivalent source $\mathbf{J}_{si}$ and the inner field $\mathbf{E}_i$ in a discretized form.

B. GIBC

From (22), $\{e_i\}$ can be expressed as

$$\{e_i\} = [K_i]^{-1}\cdot(\{V_i\} - [B_i]\{u_i\}). \quad (26)$$

Hence

$$\begin{aligned}\mathbf{E}_i &= \{\mathbf{N}_i\}^T\cdot\{e_i\}\\ &= \{\mathbf{N}_i\}^T\cdot[K_i]^{-1}\cdot(\{V_i\} - [B_i]\{u_i\})\\ &= ik_0\eta_0\{\mathbf{N}_i\}^T\cdot[K_i]^{-1}\cdot\{\mathbf{N}_i\}\cdot(\mathbf{J}_i - \mathbf{J}_{si}).\end{aligned} \quad (27)$$

There is a two-term summation in (27). The first term is called the incident field while the second term is the scattered field. They are represented as the following formats:

$$\mathbf{E}_i^{\text{inc}}(\mathbf{r}) = ik_0\eta_0\{\mathbf{N}_i\}^T\cdot[K_i]^{-1}\cdot\{\mathbf{N}_i\}\cdot\mathbf{J}_i(\mathbf{r}') \quad (28)$$

$$\mathbf{E}_i^{\text{sca}}(\mathbf{r}) = -ik_0\eta_0\{\mathbf{N}_i\}^T\cdot[K_i]^{-1}\cdot\{\mathbf{N}_i\}\cdot\mathbf{J}_{si}(\mathbf{r}'). \quad (29)$$

According to the definition of $\mathbf{M}_{si}$, we have

$$\begin{aligned}\mathbf{M}_{si} &= -\hat{n}_i\times\mathbf{E}_i\\ &= -\hat{n}_i\times(ik_0\eta_0\{\mathbf{N}_i\}^T\cdot[K_i]^{-1}\cdot\{\mathbf{N}_i\}\cdot(\mathbf{J}_i - \mathbf{J}_{si})).\end{aligned} \quad (30)$$

The aforementioned equation has connected $\mathbf{M}_{si}$ with $\mathbf{J}_{si}$. Equation (30) is essentially the GIBC. Thereby, the generalized impedance operator is defined as

$$\mathtt{Z}_i(\mathbf{r},\mathbf{r}') = ik_0\eta_0\hat{n}_i\times\{\mathbf{N}_i\}^T\cdot[K_i]^{-1}\cdot\{\mathbf{N}_i\}\quad\text{when}\ \mathbf{J}_i = 0. \quad (31)$$

We know that the scattered field $\mathbf{E}_i^{\text{sca}}$ can be expressed by the electric current $\mathbf{J}_{si}$ in the IE according the Schelkunoff equivalence principle [25]

$$\mathbf{E}_i^{\text{sca}}(\mathbf{r}) = ik_0\eta_0\int_s\bar{\mathbf{G}}_i(\mathbf{r},\mathbf{r}')\bullet[-\mathbf{J}_{si}(\mathbf{r}')]\,d\mathbf{r}' \quad (32)$$

where $\bar{\mathbf{G}}_i(\mathbf{r},\mathbf{r}')$ is the dyadic Green's function in Ω_i with the perfect magnetic conductor (PMC) boundary condition. Because of the inhomogeneity in Ω_i and arbitrary PMC boundary shape, $\bar{\mathbf{G}}_i(\mathbf{r},\mathbf{r}')$ does not have a closed-form expression. Hence, (29) also provides a numerical approach to calculate Green's function operator $\bar{\mathbf{G}}_{\mathbf{i}}(\mathbf{r},\mathbf{r}')$.

IV. Numerical Implementation

By substituting (30) into (9)–(12) or (13), we obtain a reduced representation only involving unknown $\mathbf{J}_{si}$. Taking (9) as an example, the reduced formulation is

$$\left[\mathbf{E}_0^{\text{inc}} + \eta_0\mathtt{L}\left(\sum_{i=1}^{N}\mathbf{J}_{si}\right) - \mathtt{K}\left(\sum_{i=1}^{N}\mathtt{Z}_i(\mathbf{r},\mathbf{r}')\cdot\mathbf{J}_{si}\right)\right]_{\tan} = 0. \quad (33)$$

Expanding $ik_0\eta_0\mathbf{J}_{si}$ with the RWG basis function, we get

$$\begin{aligned}&\mathtt{K}(\mathtt{Z}_i(\mathbf{r},\mathbf{r}')\cdot\mathbf{J}_{si})\\ &= \mathtt{K}(-\hat{n}_i\times\{\mathbf{N}_i\}^T\cdot[K_i]^{-1}\cdot(\{V_i\} - [B_i]\{u_i\}))\\ &= \mathtt{K}(\{\mathbf{S}_i\})\cdot[\{\mathbf{S}_i\}\cdot\{\mathbf{S}_i\}^T]^{-1}\cdot[\{\mathbf{S}_i\}^T\cdot(-\hat{n}_i\times\{\mathbf{N}_i\}^T)]\\ &\quad\cdot[K_i]^{-1}\cdot(\{V_i\} - [B_i]\{u_i\}).\end{aligned} \quad (34)$$

If we define

$$[G_i] = \{\mathbf{S}_i\}\cdot\{\mathbf{S}_i\}^T,\ \text{i.e.,}\ [G_i]_{mn} = \int_{S_i}\mathbf{S}_{im}\cdot\mathbf{S}_{in}dS \quad (35)$$

$$[H_i] = [\hat{n}_i\times\{\mathbf{S}_i\}]\cdot\{\mathbf{N}_i\}^T,\ \text{i.e.,}\ [H_i]_{mn} = \int_{S_i}(\hat{n}_i\times\mathbf{S}_{im})\cdot\mathbf{N}_{in}dS. \quad (36)$$

TABLE I
MEMORY REQUIREMENT OF EACH INTERNAL MATRIX

$[B_i]$	$[K_i]$	$[H_i]$	$[G_i]$	$[P]$ and $[Q]$
$O(L_i)$	$O(N_i)$	$O(L_i)$	$O(L_i)$	$O(L^2)$ or $O(L\log_2 L)$

Then

$$\mathtt{K}(\mathtt{Z}_i(\mathbf{r},\mathbf{r}')\cdot\mathbf{J}_{si}) = \mathtt{K}(\{\mathbf{S}_i\})\cdot[G_i]^{-1}\cdot[H_i]\cdot[K_i]^{-1} \cdot(\{V_i\}-[B_i]\{u_i\}). \quad (37)$$

Matching the boundary condition at all boundaries S_i with Galerkin method [40], a set of matrix equations are obtained as

$$\left\langle\{\mathbf{S}_j\},\sum_{i=1}^{N}\eta_0\mathbf{L}(\{\mathbf{S_i}\})+\mathtt{K}(\{\mathbf{S_i}\})\cdot[\mathbf{G_i}]^{-\mathbf{1}} \cdot[H_i]\cdot[K_i]^{-1}\cdot[B_i]\cdot\{u_i\}\right\rangle$$
$$=\left\langle\{\mathbf{S}_j\},-\mathbf{E}_0^{\mathrm{inc}}+\sum_{i=1}^{N}\mathtt{K}(\{\mathbf{S}_i\})\cdot[G_i]^{-1}\cdot[H_i]\cdot[K_i]^{-1}\cdot\{V_i\}\right\rangle, \quad j=1,2,\ldots,N. \quad (38)$$

Finally, we get a full dense matrix equation

$$[Z]\cdot\{u\}=\{V\},\{u\}=(\{u_1\}^T,\{u_2\}^T,\ldots\{u_N\}^T)^T \quad (39)$$

where

$$[Z]=[Q]+[P]\,[T] \quad (40)$$
$$\{V\}=\{V_0\}+[P]\left\{\tilde{V}\right\} \quad (41)$$
$$[Q]=\left\langle\{\mathbf{S}_j\},\sum_{i=1}^{N}\eta_0\mathtt{L}(\{\mathbf{S}_i\})\right\rangle \quad (42)$$
$$[P]=\left\langle\{\mathbf{S}_j\},\sum_{i=1}^{N}\mathtt{K}(\{\mathbf{S}_i\})\right\rangle \quad (43)$$
$$\{V_0\}=-\left\langle\{\mathbf{S}_j\},\mathbf{E}_0^{\mathrm{inc}}\right\rangle \quad (44)$$

where $[T]$ is a block diagonal matrix and $\{\tilde{V}\}$ is a block vector. Each block of them is expressed by

$$[T_i]=[G_i]^{-1}\cdot[H_i]\cdot[K_i]^{-1}\cdot[B_i] \quad (45)$$
$$\{\tilde{V}_i\}=[G_i]^{-1}\cdot[H_i]\cdot[K_i]^{-1}\{V_i\},\quad i=1,2,\ldots,N. \quad (46)$$

The internal products in (42)–(44) are defined by $\langle\{\mathbf{S}_j\},\{\mathbf{S}_i\}\rangle_{mn}=\int_S\mathbf{S}_{jm}\cdot\mathbf{S}_{in}dS$ and $\langle\{\mathbf{S}_j\},\mathbf{E}_0^{\mathrm{inc}}\rangle_m=\int_S\mathbf{S}_{jm}\cdot\mathbf{E}_0^{\mathrm{inc}}dS$, where subscripts m and n corresponds to the element at mth row and nth column in each matrix or vector.

As a brief analysis, the memory requirement of each internal matrix in (39) is shown in Table I. And Table II shows the computational complexity (CPU time cost) of each step to solve the final system matrix.

Matrices $[G_i]$, $[H_i]$, $[K_i]$, and $[B_i]$are extremely sparse. The memory cost of a sparse matrix with the bandwidth W and dimension M is about $O(WM)$. $[Q]$ and $[P]$ are fully dense matrices. Their storage requirement is $O(L^2)$ for method of moment and can be reduced to $O(L\log_2 L)$ with the MLFMA for electrically large objects, where$L=\sum_{i=1}^{N}L_i$.

TABLE II
COMPUTATIONAL COMPLEXITY OF EACH STEP TO SOLVE THE SYSTEM MATRIX

Matrix Equation: $([Q]+[P][T])\{u\}=\{V\}$			
Direct Solution (LU)		Iterative Solution	
$[Z_1]=[K_i]^{-1}[B_i]$	$O(L_iN_i)$	$\{x_1\}=[B_i]\{u\}$	$O(L_i)$
$[Z_2]=[H_i][Z_1]$	$O(L_i^2)$	$\{x_2\}=[K_i]^{-1}\{x_1\}$	$O(N_i)$
$[Z_3]=[G_i]^{-1}[Z_2]$	$O(L_i^2)$	$\{x_3\}=[H_i]\{x_2\}$	$O(L_i)$
$[Z]=[Q]+[P][Z_3]$	$O(L_i^2)$	$\{x_4\}=[G_i]^{-1}\{x_3\}$	$O(L_i)$
$\{u\}=[Z]^{-1}\{V\}$	$O(L^3)$	$\{x_5\}=[Q]\{u\}+[P]\{x_4\}$	$O(L^2)$ or $O(L\log_2 L)$

The computational complexity for inversing a sparse matrix with bandwidth W and dimension M is about $O(W^2M)$. Usually, the bandwidth of a finite element matrix is quite small, especial compared with its dimension. Thus, both the memory requirement and computational complexity of $[G_i]$/$[K_i]$can be approximated to $O(L_i)$/$O(N_i)$. Therefore, by using the direct LU decomposition provided in software packages such as the MUMPS [29], it is very efficient to get the value of $[X]$ by solving a submatrix equation $[A][X]=[Y]$. Since $[H_i]$ and $[B_i]$ are sparse matrices, they are efficient for matrix–vector multiplications. The computational cost for each matrix–vector multiplication is about $O(L_i)$. Matrices $[Q]$ and $[P]$ are fully dense. To solve the final system matrix, the computational complexity is at $O(L^3)$ and $O(L^2)$ for direct solution and iterative solution, respectively. Fortunately, for electrically large objects, the computational effort for matrix–vector multiplications can be reduced to $O(L\log_2 L)$ with the MLFMA as well. Even if the iterative solver hardly converges for some special problem, (39) still can be efficiently solved with LU decomposition because the matrix dimension L is relative small owing to only surface unknowns $\mathbf{J}_{si}$ are involved. After getting $\{u_i\}$, vector $\{e_i\}$ is available by (26). Then, the calculation of near field is quite efficient by (20). The far field can be computed with source-field transformation in integral (1)–(4).

V. PLASMONIC NANOSTRUCTURE SIMULATION

To demonstrate the validity and efficiency of our proposed FEM-GIBC method for the plasmonic simulation, two plasmonic nanostructures are modeled and investigated.

In the first benchmark, a system consisting of two gold nanospheres is calculated to analyze the local surface plasmon enhancement. Two nanospheres are closely packed along x-direction in the free space. The diameter of each nanosphere is 15 nm and the spacing between them is 1.5 nm. An x-polarized light along z-direction illuminates these spheres. The complex permittivity (or refractive index) of gold is taken by the Brendel–Bormann (BB) model that can capture both the free-electron and interband parts of the dielectric response of metals in a wide spectral range from 0.1 to 6 eV [41]. The bulk parameter of

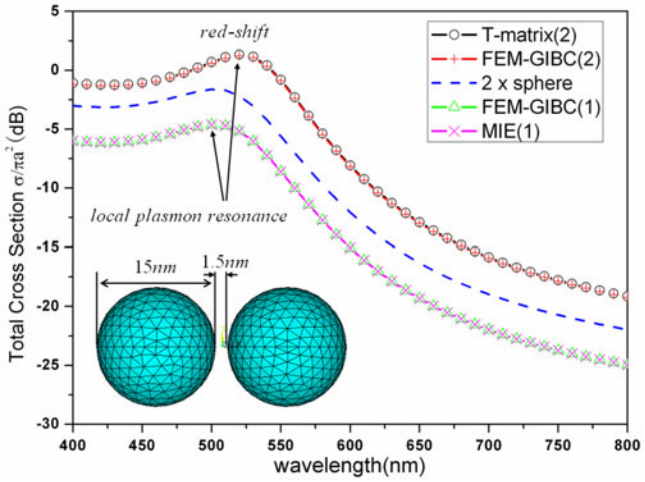

Fig. 3. TCS of single and double gold nanospheres with diameter of 15 nm. The spacing of double spheres is 1.5 nm.

permittivity by the BB model validates for very small nanoparticles until the size smaller than 5 nm, where quantum effects arise. In the visible light frequency band, the total cross section (TCS) is calculated by the optical theorem [42]

$$\sigma_{\rm tcs} = \frac{4\pi}{k}{\rm Im}[\hat{e}_i \cdot \bar{\mathbf{F}}(\hat{k}_i, \hat{k}_i) \cdot \hat{e}_i] \tag{47}$$

$$\mathbf{E}^{\rm sca}(\mathbf{r}) = \frac{e^{ik|\mathbf{r}|}}{|\mathbf{r}|}\bar{\mathbf{F}}(\hat{k}_s, \hat{k}_i) \cdot \hat{e}_i |\mathbf{E}^{\rm inc}|. \tag{48}$$

Here, $\sigma_{\rm tcs}$ represents the total cross section which indicates the total energy loss from the incident wave due to the scattering and absorption of a wave by the scatterer. $\bar{\mathbf{F}}(\hat{k}_i, \hat{k}_i)$ is the scattering dyad in the scattered direction $\hat{k}_s$ for the incident wave in the direction $\hat{k}_i$. Here, $\hat{e}_i$ denotes the polarization of the incident plane wave. We know that the lifetime of plasmon resonance is fundamentally limited by its intrinsic loss including both the scattering and absorption loss [43], [44]. On the basis of the uncertainty principle $\Delta\omega\Delta t \geq 1/2$, the simulated half power bandwidth of the TCS can be useful for estimating the lifetime of plasmon resonance.

The simulation results are shown in Fig. 3. The reference results of the single and double spheres are calculated with Mie series and the T-matrix method, respectively. We can see that the simulated results by FEM-GIBC almost coincide with the references. Due to the evanescent wave coupling, the plasmonic resonance of the close-packed double nanospheres is red shifted in comparison to the single nanosphere and the value of $\sigma_{\rm tcs}$ is even larger than two times that of the single sphere, which is plotted in dashed line. Fig. 4(a) and (b) shows the near-field profile of the single sphere and double spheres at resonance. The field value is normalized and the logarithmic color is adopted. Then, the value between -60 and 0 dB is scaled and shifted to 0–1 dB. As shown in Fig. 4, the single nanosphere is essentially a dipole emitter and the dipole–dipole coupling between the sphere dimer significantly enhances the near field in the sphere gap.

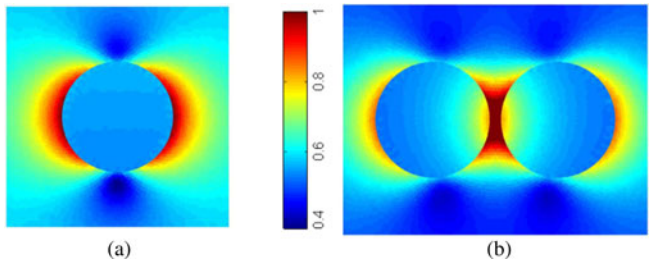

Fig. 4. Near-field distribution at resonance. (a) Single sphere. (b) Double spheres.

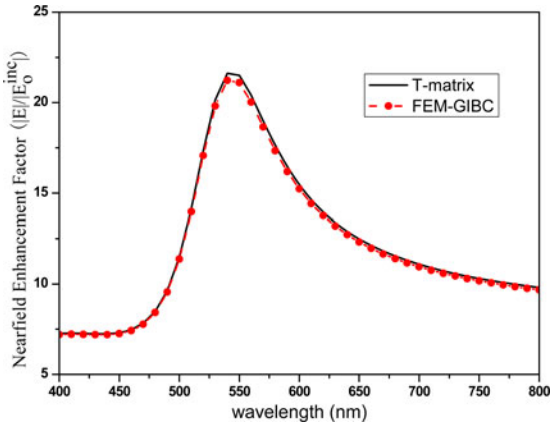

Fig. 5. Near-field enhancement factor at center point (0, 0, 0) as a function of the frequency.

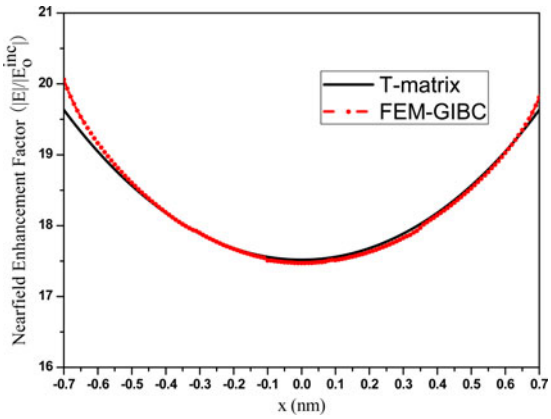

Fig. 6. Near-field distribution in the gap of two nanospheres at wavelength 520 nm.

Figs. 5 and 6 show the accuracy comparisons of near-field simulation between FEM-GIBC and T-matrix methods. The calculated near-field enhancement factor, which is defined by $Q = |\mathbf{E}| \,/\, |\mathbf{E}_0^{\rm inc}|$, agrees well with the analytical ones. The ability to accurately capture the near-field physics of the proposed method is strongly confirmed. The convergence property is shown in Fig. 7, where the relative error of near fields defined by ${\rm err} = |\mathbf{E} - \mathbf{E}_{\rm ref}| \,/\, |\mathbf{E}_{\rm ref}|$ is illustrated. $\mathbf{E}_{\rm ref}$ denotes the analytical value by T-matrix method. As the average grid size decrease from 1.5 to 0.5 nm, equivalently, the number of unknowns increase from 1908 to 18324, the relative error goes to smaller and smaller.

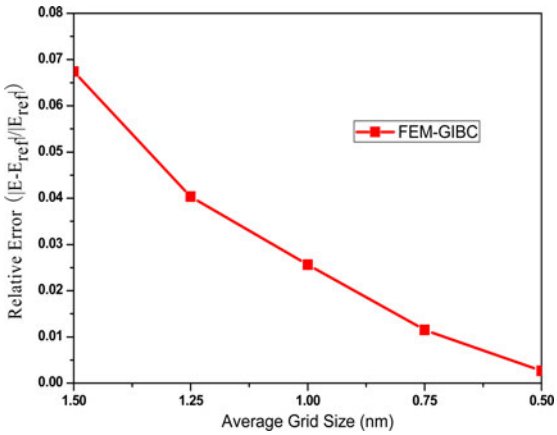

Fig. 7. Convergence rate of relative error of near fields. T-matrix solution is adopted as a reference solution.

For the wideband calculation (400 to 800 nm), we simulated the nanostructures at 41 sampling frequency points with interval 10 nm. Due to the geometric similarity, we mesh the two spheres with basic elements as a two-region problem. Only one GIBC needs to be established at sphere's interface, the GIBC at others has the same expression. Hence, the setup time can be reduced dramatically. Therefore, the proposed method is most efficient for electromagnetic simulation of finite periodic structures. In this benchmark, finite element discretization give rise to 28124 basis functions in each region, while the dimension of the final system matrix is only 1908. With running our code on a workstation with 32 threads and solving the system matrix with LU decomposition, the peak value of memory occupation is about 240 M byte and the CPU time cost is less than 1 min for each sampling point. After getting the solution of system matrix, (20) is adopted in the internal regions, and surface integral formulations are used at the exterior region to obtain the near-field distribution with negligible efforts.

The second example simulates the thin-film plasmonic solar cells. Figs. 8(a) and 9(a) illustrate the schematic patterns of the bulk heterojunction organic solar cell (OSC). The active layer is a blend polymer of P3HT(poly(3-hexylthiophene)) and PCBM (methanofullerene). The hole conduction layer is PEDOT: PSS(poly(3,4-ethyenedioxythiophene):poly(4-styrenesulfonic acid)) which is chosen as an optical spacer between the electrode and the active layer. Four Ag nanocubes are embedded into the polymer layers as field concentrators. The complex refraction index of polymers and silver are available in literatures [41], [45]. The incident light with x polarization is propagated from the spacer layer to the active layer. In this benchmark, the absorption of active layer is investigated when the concentrators are embedded in the spacer layer and the active layer, respectively. The absorption can be calculated by

$$\sigma_{\rm abs} = \int \sigma \left|\mathbf{E}\right|^2 dV \tag{49}$$

where σ is the optical conductivity of the active material. The optical enhancement factor can be obtained by the ratio of the

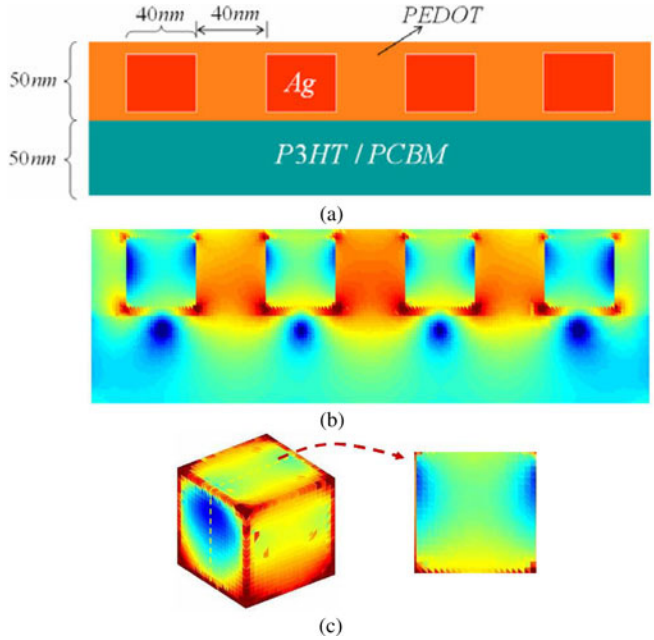

Fig. 8. Schematic pattern and the near-field distribution of OSC nanostructures when the concentrators are embedded in the spacer layer. (a) Schematic pattern. (b) Near-field distribution in the longitudinal profile. (c) Surface field distribution for the Ag cube.

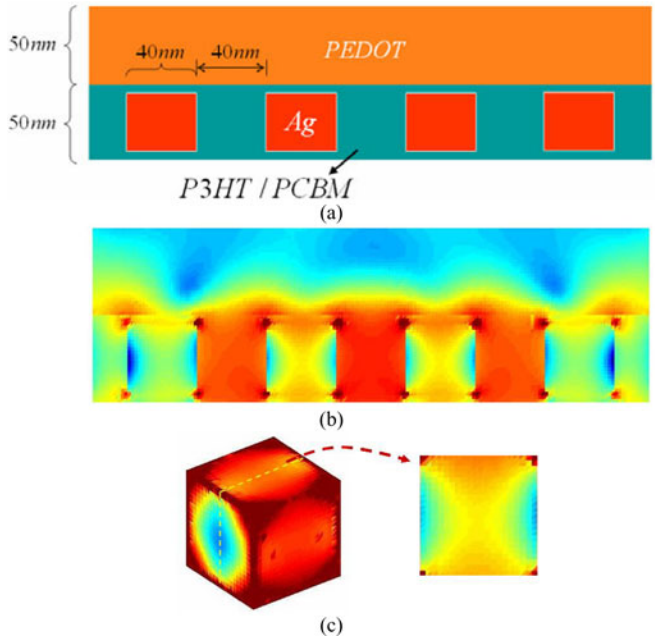

Fig. 9. Schematic pattern and the near-field distribution of OSC nanostructures when the concentrators are embedded in the active layer. (a) Schematic pattern. (b) Near-field distribution in the longitudinal profile. (c) Surface field distribution for the Ag cube.

absorption with concentrators over that without the concentrators.

The FEM-GIBC method generates 326 012 finite element basis functions and 4608 RWG basis functions which are utilized to express the equivalent current. The memory requirement is about 2 G byte and each sampling point takes about 4 min to solve the system matrix with iteration method. Figs. 8(b) and

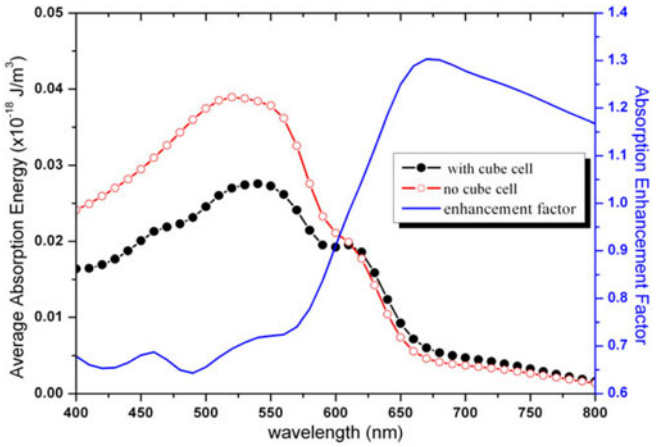

Fig. 10. Average absorption energy and the absorption enhancement factor as a function of wavelength when the nanocube concentrators are embedded in the spacer layer.

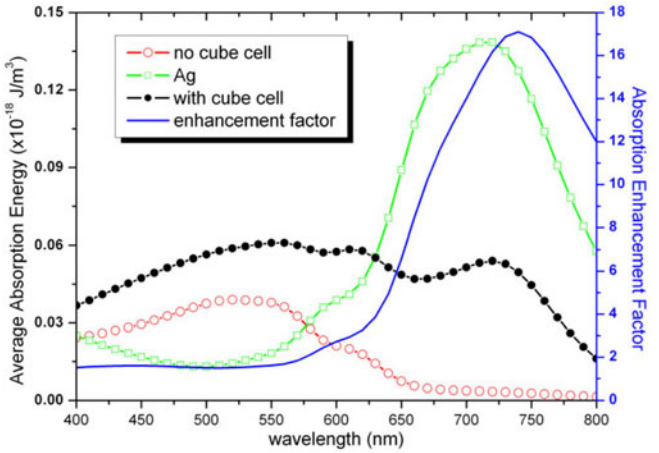

Fig. 11. Average absorption energy and the absorption enhancement factor as a function of wavelength when the nanocube concentrators are embedded in the active layer.

9(b) show the near-field distributions in the OSC at the peaks of the absorption enhancement.

The electric field is noticeably enhanced in the neighborhood of each nanocube. Due to the significant difference of refraction indices, the electric field has a jump at the interface between Ag and background media. When the concentrators are embedded in the spacer layer, the nanocubes block the light, and absorb most of the energy. Only little light energy can penetrate into the active medium. Hence, the optical absorption enhancement in the active region is very small. However, when the Ag nanocubes are embedded into the active layer, the optical absorption of the active layer is substantially improved. The enhanced near E-field by the plasmonic nanocubes can be directly and sufficiently absorbed by the contiguous active medium. The electric field distributions at the surfaces of nanocubes are shown in Figs. 8(c) and 9(c). The field at the interface is very strong and decays rapidly in the metal because of the high conductive loss.

Figs. 10 and 11 show the average absorption energy and absorption enhancement factor as a function of wavelength. When the concentrators are embedded in the active layer, the energy absorbed by silver cubes is also shown in Fig. 11. Although silver cubes show large metallic loss, the absorption of the active medium still can be significantly enhanced because of the plasmon resonances, especially at the long wavelength region. It was worth mentioning that the accuracy of our calculation results has been verified by the h-adaptive scheme. That is, the simulated result always converges to the same values when we refine the mesh of geometry.

VI. Conclusion

This paper has proposed a novel GIBC based on the FEM to simulate plasmonic nanostructures. At first, the scattering from nanostructures is equivalent to the radiation from equivalent sources on boundaries according to the equivalence principle. The BIE is established using both electric equivalent currents and magnetic equivalent currents. After that, to determine the unique solution of the BIE, the GIBC is formulated based on the FEM. A GIBC connecting magnetic equivalent currents and electric equivalent currents is established. Hence, the BIE is reformatted to contain only unknown electric equivalent currents. Then, it is converted to a matrix equation and solved through the basis function expansion and the Galerkin testing method.

Subwavelength tetrahedrons and triangular patches are used to mesh the nanostructures and their boundaries. The inner electric field and boundary equivalent sources are represented by the second-order finite element basis functions and RWG basis functions, respectively. The numerical matrices generated by the FEM are extremely sparse. Hence, the MUMPS is adopted to complete their inverse. Although the BIEs give rise to full dense matrices, they can be efficiently solved with the MLFMA. Even if the iterative solver hardly converges for some special problems, the final matrix still can efficiently be solved with LU decomposition because the matrix dimension is relative small owing to only electric equivalent currents are involved. Hence, the proposed simulation method is very powerful and its computer resource requirement is low. The proposed method has significant advantages over commonly used DDA, finite difference method, SIE, etc.

Based on the proposed approach, several plasmonic nanostructures are modeled and simulated. The plasmon enhancement and their applications in OSC have been analyzed. This FEM-GIBC is a general numerical approach, which can be utilized to simulate any nanostructure with arbitrary inhomogeneity and shapes. They can provide accurate and efficient near-field simulation for the plasmonic nanostructures.

Acknowledgment

The authors would like to thank Dr. Y. Liu from Hong Kong University, Hong Kong, for providing T-matrix reference results of nanospheres.

References

[1] A. J. Haes, W. P. Hall, L. Chang, W. L. Klein, and R. P. Van Duyne, "A localized surface plasmon resonance biosensor: First steps toward an assay for Alzheimer's disease," *Nano Lett.*, vol. 4, pp. 1029–1034, Jun. 2004.

[2] V. M. Shalaev and S. Kawata, *Nanophotonics With Surface Plasmons*. Amsterdam, The Netherlands: Elsevier, 2006.
[3] S. A. Maier, *Plasmonics: Fundamentals and Applications*. New York: Springer, 2007.
[4] S. Pillai, K. R. Catchpole, T. Trupke, and M. A. Green, "Surface plasmon enhanced silicon solar cells," *J. Appl. Phys.*, vol. 101, pp. 093105-1–093105-8, May 1, 2007.
[5] H. A. Atwater and A. Polman, "Plasmonics for improved photovoltaic devices," *Nature Mater.*, vol. 9, pp. 205–213, Mar. 2010.
[6] L. Novotny and B. Hecht, *Principles of Nano-Optics*. New York: Cambridge Univ. Press, 2006.
[7] K. Ohno, M. Tanaka, J. Takeda, and Y. E. Kawazoe, *Nano- and Micromaterials*. Berlin, Germany: Springer, vol. 9, 2008.
[8] W. C. Chew, *Waves and Fields in Inhomogenous Media*. New York: Wiley-IEEE Press, vol. 3, 1999.
[9] C. Hafner, *The Generalized Multiple Multipole Technique for Computational Electromagnetics*. Boston, MA: Artech House, 1990.
[10] K. Yee, "Numerical solution of initial boundary value problems involving Maxwell's equations in isotropic media," *IEEE Trans. Antennas Propag.*, vol. 14, no. 3, pp. 302–307, May 1966.
[11] A. Taflove and M. E. Brodwin, "Numerical-solution of steady-state electromagnetic scattering problems using time-dependent maxwells equations," *IEEE Trans. Microw. Theory Tech.*, vol. 23, no. 8, pp. 623–630, Aug. 1975.
[12] J. M. Jin, *The Finite Element Method in Electromagnetics*, 2nd ed. New York: Wiley-IEEE Press, 2002.
[13] D. H. Schaubert, D. R. Wilton, and A. W. Glisson, "A tetrahedral modeling method for electromagnetic scattering by arbitrarily shaped inhomogeneous dielectric bodies," *IEEE Trans. Antennas Propag.*, vol. 32, no. 1, pp. 77–85, Jan. 1984.
[14] J. P. Kottmann and O. J. F. Martin, "Accurate solution of the volume integral equation for high-permittivity scatterers," *IEEE Trans. Antennas Propag.*, vol. 48, no. 11, pp. 1719–1726, Nov. 2000.
[15] W. H. Yang, G. C. Schatz, and R. P. Vanduyne, "Discrete dipole approximation for calculating extinction and Raman intensities for small particles with arbitrary shapes," *J. Chem. Phys.*, vol. 103, pp. 869–875, Jul. 1995.
[16] S. Kagami and I. Fukai, "Application of boundary-element method to electromagnetic-field problems," *IEEE Trans. Microw. Theory Tech.*, vol. 32, no. 4, pp. 455–461, Apr. 1984.
[17] R. F. Harrington, "Boundary integral formulations for homogeneous material bodies," *J. Electromagn. Waves Appl.*, vol. 3, pp. 1–15, 1989.
[18] P. Yla-Oijala, "Application of a novel CFIE for electromagnetic scattering by dielectric objects," *Microw. Opt. Technol. Lett.*, vol. 35, pp. 3–5, Oct. 2002.
[19] Y. H. Chu and W. C. Chew, "Large-scale computation for electrically small structures using surface-integral equation method," *Microw. Opt. Technol. Lett.*, vol. 47, pp. 525–530, Dec. 2005.
[20] A. M. Kern and O. J. F. Martin, "Surface integral formulation for 3D simulations of plasmonic and high permittivity nanostructures," *J. Opt. Soc. Amer. A*, vol. 26, pp. 732–740, Apr. 2009.
[21] B. Engquist and A. Majda, "Absorbing boundary-conditions for numerical-simulation of waves," *Math. Comput.*, vol. 31, pp. 629–651, 1977.
[22] W. C. Chew and W. H. Weedon, "A 3d perfectly matched medium from modified Maxwells equations with stretched coordinates," *Microw. Opt. Technol. Lett.*, vol. 7, pp. 599–604, Sep. 1994.
[23] Z. Q. Zhang and Q. H. Liu, "Three-dimensional weak-form conjugate- and biconjugate-gradient FFT methods for volume integral equations," *Microw. Opt. Technol. Lett.*, vol. 29, pp. 350–356, Jun. 2001.
[24] C. C. Lu, "A fast algorithm based on volume integral equation for analysis of arbitrarily shaped dielectric radomes," *IEEE Trans. Antennas Propag.*, vol. 51, no. 3, pp. 606–612, Mar. 2003.
[25] R. F. Harrington, *Time-Harmonic Electromagnetic Fields*, 2nd ed. New York: Wiley-IEEE Press, 2001.
[26] Z. G. Qian, W. C. Chew, and R. Suaya, "Generalized impedance boundary condition for conductor modeling in surface integral equation," *IEEE Trans. Microw. Theory Tech.*, vol. 55, no. 11, pp. 2354–2364, Nov. 2007.
[27] W. C. Chew, J. M. Jin, E. Michielssen, and J. M. Song, *Fast and Efficient Algorithms in Computational Electromagnetics*. Boston, MA: Artech House, 2001.
[28] J. P. Webb, "Hierarchal vector basis functions of arbitrary order for triangular and tetrahedral finite elements," *IEEE Trans. Antennas Propag.*, vol. 47, no. 8, pp. 1244–1253, Aug. 1999.
[29] P. R. Amestoy, I. S. Duff, J. Y. L'Excellent, and J. Koster, "A fully asynchronous multifrontal solver using distributed dynamic scheduling," *SIAM J. Matrix Anal. Appl.*, vol. 23, pp. 15–41, Apr. 2001.
[30] T. Cwik, C. Zuffada, and V. Jamnejad, "Modeling three-dimensional scatterers using a coupled finite element—Integral equation formulation," *IEEE Trans. Antennas Propag.*, vol. 44, no. 4, pp. 453–459, Apr. 1996.
[31] M. M. Botha and J. M. Jin, "On the variational formulation of hybrid finite element-boundary integral techniques for electromagnetic analysis," *IEEE Trans. Antennas Propag.*, vol. 52, no. 11, pp. 3037–3047, Nov. 2004.
[32] Z. Peng and X. Q. Sheng, "A flexible and efficient higher order FE-BI-MLFMA for scattering by a large body with deep cavities," *IEEE Trans. Antennas Propag.*, vol. 56, no. 7, pp. 2031–2042, Jul. 2008.
[33] S. C. Lee, M. N. Vouvakis, K. Z. Zhao, and H. F. Lee, "Analysing microwave devices using a symmetric coupling of finite and boundary elements," *Int. J. Numerical Methods Eng.*, vol. 64, pp. 528–546, Sep. 2005.
[34] K. Z. Zhao, "A domain decomposition method for solving electrically large electromagnetic problems," Ph.D. dissertation, Dept. Electr. Comput. Eng., The Ohio State Univ., Columbus, 2007.
[35] K. Z. Zhao, V. Rawat, and J. F. Lee, "A domain decomposition method for electromagnetic radiation and scattering analysis of multi-target problems," *IEEE Trans. Antennas Propag.*, vol. 56, no. 8, pp. 2211–2221, Aug. 2008.
[36] W. H. Press, S. Teukolsky, W. Vetterling, and B. Flannery, *Numerical Recipes: The Art of Scientific Computing*, 3rd ed. New York: Cambridge Univ. Press, 2007.
[37] J. A. Stratton, *Electromagnetic Theory*. New York: McGraw-Hill, 1941.
[38] X. Q. Sheng, J. M. Jin, J. M. Song, W. C. Chew, and C. C. Lu, "Solution of combined-field integral equation using multilevel fast multipole algorithm for scattering by homogeneous bodies," *IEEE Trans. Antennas Propag.*, vol. 46, no. 11, pp. 1718–1726, Nov. 1998.
[39] S. M. Rao, D. R. Wilton, and A. W. Glisson, "Electromagnetic scattering by surfaces of arbitrary shape," *IEEE Trans. Antennas Propag.*, vol. 30, no. 3, pp. 409–418, May 1982.
[40] R. F. Harrington, *Field Computation by Moment Methods*. New York: Wiley-IEEE Press, 1993.
[41] A. D. Rakic, A. B. Djurišic, J. M. Elazar, and M. L. Majewski, "Optical properties of metallic films for vertical-cavity optoelectronic devices," *Appl. Opt.*, vol. 37, pp. 5271–5283, 1998.
[42] L. Tsang, J. A. Kong, and K.-H. Ding, *Scattering of Electromagnetic Waves: Theories and Applications*. New York: Wiley-Interscience, 2000.
[43] A. Politano and G. Chiarello, "Tuning the lifetime of the surface plasmon upon sputtering," *Phys. Status Solidi-Rapid Res. Lett.*, vol. 3, pp. 136–138, 2009.
[44] Y.-F Chau, Z.-H. Jiang, H.-Y. Li, G.-M. Lin, F.-. Wu, and W.-H. Lin, "Localized resonance of composite core-shell nanospheres, nanobars and nanospherical chains," *Prog. Electromagn. Res. B*, vol. 28, pp. 183–199, 2011.
[45] W. C. H. Choy and H. H. Fong, "Comprehensive investigation of absolute optical properties of organic materials," *J. Phys. D-Appl. Phys.*, vol. 41, pp. 155109-1–155109-7, Aug. 2008.

Shiquan He (S'08) was born in Sichuan, China, in 1984. He received the B.S. degree in electromagnetics and microwave technology from the University of Electronic Science and Technology of China, Chengdu, China, in 2006, where he is currently working toward the Ph.D. degree.

Since October 2009, he has been a Visiting Researcher in the Electromagnetics and Optics Research Group, Department of Electrical and Electronic Engineering, the University of Hong Kong, Hong Kong. His research interests include finite element methods, integral equation methods, and fast algorithms in computational electromagnetics.

Wei E. I. Sha (M'09) was born in Suzhou, China, in 1982. He received the B.S. and Ph.D. degrees in electronic engineering from Anhui University, Hefei, China, in 2003 and 2008, respectively.

He is currently a Postdoctoral Research Fellow with the Department of Electrical and Electronic Engineering, the University of Hong Kong, Hong Kong. He has authored or coauthored more than 20 referred papers, one book chapter, and one book. His current research interests include electromagnetics, nanooptics, and modern signal processing.

Lijun Jiang (S'01–M'04) received the B.S. degree in electrical engineering from the Beijing University of Aeronautics and Astronautics, Beijing, China, in 1993, the M.S. degree from the Tsinghua University, Beijing, in 1996, and the Ph.D. degree from the University of Illinois at Urbana-Champaign, Urbana-Champaign, in 2004.

From 1996 to 1999, he was an Application Engineer with the Hewlett-Packard Company. Since 2004, he has been a Postdoctoral Researcher, the Research Staff Member, and the Senior Engineer at IBM T. J. Watson Research Center, Yorktown Heights, NY. Since the end of 2009, he has also been an Associate Professor with the Department of Electrical and Electronic Engineering, the University of Hong Kong, Hong Kong. His research interests include electromagnetics, IC signal/power integrity, antennas, multidisciplinary electronic design automation solutions, RF and microwave technologies, and high-performance computing.

He received the IEEE Microwave Theory Techniques Graduate Fellowship Award in 2003 and the Y. T. Lo Outstanding Research Award in 2004. He is a member of the IEEE Antennas and Propagation Society, and an Associate member of the Sigma Xi. He was the Semiconductor Research Cooperation (SRC) Industrial Liaison for several academic projects. Since 2009, he has been the SRC Packaging High Frequency Topic TT Chair. He also serves as the Reviewer of the IEEE Transactions on several topics, and other primary electromagnetics and microwave related journals.

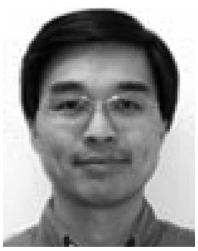

Wallace C. H. Choy (SM'09) received the Ph.D. degree in electronic engineering from the University of Surrey, U.K., in 1999.

His work at Surrey was supported by the Croucher Foundation Scholarship. He then joined National Research Council of Canada as a member of research staff to work on optical device structures of polarization independent optical amplifiers and modulators. He joined Fujitsu at San Jose, U.S. in 2001 to develop real-time wavelength tunable lasers and optical transmitter modules. He is now an Associate Professor of the Department of Electrical and Electronic Engineering, University of Hong Kong (HKU). His current research interests are concerned with organic optoelectronic devices, plasmonic structures and nano-material devices. He has published over 95 internationally peer-reviewed journal papers, contributed to two book chapters, US and China patents.

Dr. Choy was the recipient of the Sir Edward Youde Memorial Fellowship, the Croucher Foundation Fellowship, and the Outstanding Achievement Award from National Research Council of Canada. He received overseas visiting fellowships from HKU to take a sabbatical leave at George Malliaras's Group, Cornell University in 2008, a visit to Prof. Y. Yang, UCLA in summers of 2009 and 2011, and a visit to Prof. Karl Leo, Institut fuer Angewandte Photophysik (IAPP), Technische Universitaet Dresden, Germany in the summer of 2010 for studying organic LEDs and solar cells. He has been serving a technical consultant of HK-Ulvac (a member of stock-listed Ulvac Corp) since 2005. He has delivered a number of invited talks and served as a committee member in internationally industrial and academic conferences organized by various organizations such as IEEE, OSA and Plastic Electronics Foundation.

Weng Cho Chew (S'79–M'80–SM'86–F'93) received the B.S. degree in 1976, both the M.S. and Engineer's degrees in 1978, and the Ph.D. degree in 1980, all in electrical engineering from the Massachusetts Institute of Technology, Cambridge.

He is serving as the Dean of Engineering at The University of Hong Kong, Hong Kong. He was a Professor and the Director of the Center for Computational Electromagnetics and the Electromagnetics Laboratory, the University of Illinois at Urbana-Champaign, Urbana-Champaign. Before joining the University of Illinois at Urbana-Champaign, he was the Department Manager and a Program Leader at Schlumberger-Doll Research, Cambridge. He is the originator of several fast algorithms for solving electromagnetics scattering and inverse problems. He has led a research group that has developed parallel codes to solve dense matrix systems with tens of millions of unknowns for the first time for integral equations of scattering. He has authored a book entitled *Waves and Fields in Inhomogeneous Media* (New York: IEEE Press, 1999), coauthored two books entitled *Fast and Efficient Methods in Computational Electromagnetics* (Boston, MA: Artech House, 2001) and *Integral Equation Methods for Electromagnetic and Elastic Waves* (1st ed. San Rafael, CA: Morgan & Claypool Publishers, 2007), authored or coauthored more than 300 journal publications, more than 400 conference publications, and more than ten book chapters. His research interests include the areas of waves in inhomogeneous media for various sensing applications, integrated circuits, microstrip antenna applications, and fast algorithms for solving wave scattering and radiation problems.

Dr. Chew served on the IEEE Adcom for Antennas and Propagation Society as well as on the Geoscience and Remote Sensing Society. He has been active with various journals and societies. He is the Fellow of the Optical Society of America, Institute of Physics, Electromagnetics Academy, Hong Kong Institute of Engineers, and was the National Science Foundation Presidential Young Investigator. He received the Schelkunoff Best Paper Award for Antennas and Propagation (AP) Transaction, the IEEE Graduate Teaching Award, the UIUC Campus Wide Teaching Award, and the IBM Faculty Awards. He was a Founder Professor of the College of Engineering, and previously, the First Y. T. Lo Endowed Chair Professor in the Department of Electrical and Computer Engineering, the University of Illinois at Urbana-Champaign. From 2005 to 2007, he served as an IEEE Distinguished Lecturer. He served as the Cheng Tsang Man Visiting Professor at Nanyang Technological University, Singapore, in 2006. In 2002, the Institute for Science Information Citation elected him to the category of most highly cited authors (top 0.5%). In 2008, he was elected by the IEEE AP Society to receive the Chen-To Tai Distinguished Educator Award. He is currently the Editor-in-Chief of the *Journal of Electromagnetic Waves and Applications*/*Progress in Electromagnetic Research Journal*, and on the Board of Directors of Applied Science Technology Research Institute, Hong Kong.

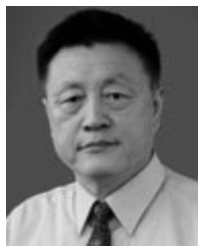

Zaiping Nie (SM'96) was born in Xi'an, China, in 1946. He received the B.S. degree in radio engineering and the M.S. degree in electromagnetic field and microwave technology from the Chengdu Institute of Radio Engineering (now University of Electronic Science and Technology of China), Chengdu, China, in 1968 and 1981, respectively.

From 1987 to 1989, he was a Visiting Scholar with the Electromagnetics Laboratory, The University of Illinois at Urbana-Champaign, Urbana-Champaign. He is currently a Professor in the Department of Microwave Engineering, University of Electronic Science and Technology of China. He has published more than 300 journal papers. His research interests include antenna theory and techniques, fields and waves in inhomogeneous media, computational electromagnetics, electromagnetic scattering and inverse scattering, new techniques for antenna in mobile communications, and transient electromagnetic theory and applications.